BJR

■ BONE FRACTURE

Alcohol-induced inhibition of bone formation and neovascularization contributes to the failure of fracture healing via the miR-19a-3p/FOXF2 axis

D. Zhu,
H. Fang,
H. Yu,
P. Liu,
Q. Yang,
P. Luo,
C. Zhang,
Y. Gao,
Y-X. Chen

From Shanghai Jiao Tong University Affiliated Sixth People's Hospital, Shanghai, China

Aims

Alcoholism is a well-known detrimental factor in fracture healing. However, the underlying mechanism of alcohol-inhibited fracture healing remains poorly understood.

Methods

MicroRNA (miR) sequencing was performed on bone mesenchymal stem cells (BMSCs). The effects of alcohol and miR-19a-3p on vascularization and osteogenic differentiation were analyzed in vitro using BMSCs and human umbilical vein endothelial cells (HUVECs). An in vivo alcohol-fed mouse model of femur fracture healing was also established, and radiological and histomorphometric analyses were used to evaluate the role of miR-19a-3p. The binding of miR-19a-3p to forkhead box F2 (FOXF2) was analyzed using a luciferase reporter assay.

Results

miR-19a-3p was identified as one of the key regulators in the osteogenic differentiation of BMSCs, and was found to be downregulated in the alcohol-fed mouse model of fracture healing. In vitro, miR-19a-3p expression was downregulated after ethanol administration in both BMSCs and HUVECs. Vascularization and osteogenic differentiation were independently suppressed by ethanol and reversed by miR-19a-3p. In addition, the luciferase reporter assay showed that FOXF2 is the direct binding target of miR-19a-3p. In vivo, miR-19a-3p agomir stimulated callus transformation and improved the alcohol-impaired fracture healing.

Conclusion

This study is the first to demonstrate that the miR-19a-3p/FOXF2 axis has a pivotal role in alcohol-impaired fracture healing, and may be a potential therapeutic target.

Article focus

■ This article focuses on the role of microRNA (miR)-19a-3p/forkhead box F2 (FOXF2) in alcohol-impaired fracture healing.

Key messages

■ miR-19a-3p agomir can stimulate callus transformation and ameliorate alcohol-inhibited fracture healing.

Strengths and limitations

■ This study is the first to demonstrate that the miR-19a-3p/FOXF2 axis has a pivotal

role in alcohol-impaired fracture healing and may be a potential therapeutic target.

■ Future clinical trials are needed to verify the current findings.

■ The mechanism of miR-19a-3p on the vascularization needs to be further clarified.

Introduction

Bone fractures are one of the most common injuries of the musculoskeletal system.[1,2] Failed healing, manifesting as delayed union or nonunion, can occur in 5% to 10% of all fractures.[3,4] To reduce costs and improve

Correspondence should be sent to Youshui Gao; email: gaoyoushui@sjtu.edu.cn

fracture care in these cases, novel therapies to promote fracture healing need to be developed.[5] Fracture healing is influenced by many factors, including age, smoking, concomitant diseases, and the energy of the injury.[6-9]

Chronic and heavy alcohol consumption can disturb the bone homeostasis, which may eventually lead to an increased likelihood of fracture nonunion or delayed union.[10,11] An increasing number of clinical studies have reported the detrimental effects of alcohol abuse on fracture healing.[12,13] Several animal studies on alcohol exposure and bone health have reported similar results.[14,15] The mechanisms are complex and involve the bone cells, endocrine system, pancreas, and cytokine system.[16] However, insufficient attention has been paid to the pathogenic mechanisms and potential therapeutic strategies.

Fracture healing requires the coordinated occurrence of bone formation and neovascularization.[2,17] After the injury, a fracture haematoma appears in the fracture site. Immediately thereafter, granulation tissue begins to form and hypoxia initiates the transformation of bone marrow mesenchymal stem cells (BMSCs) into hypertrophic chondrocytes and the formation of soft callus.[18,19] Subsequently, in situ neovascularization provides essential oxygen and nutrients, resulting in the apoptosis and transdifferentiation of the hypertrophic chondrocytes into osteoblasts and the activation of osteoclasts, and directly drives the maturation and remodelling process of bone callus.[20-22] In this process, the formation of new vessels primarily facilitates oxygen and nutrient delivery. The maturation of a soft callus into a hard callus relies on the invasion of new blood vessels, whereas the process of callus maturation produces sufficient vascular endothelial growth factor (VEGF) to support the neighbouring newly formed vessels.[23] Clinical evidence shows that poor vascularity at the fracture site is a risk factor for fracture nonunion.[24] Chen et al[25] demonstrated the deteriorating effect of alcohol on the coupling of osteogenesis and angiogenesis in skeletal tissue, which leads to the development of osteoporosis. Recent studies also support the hypothesis that alcohol exposure impairs both the osteogenic differentiation of BMSCs and the process of neovascularization.[26,27] However, the inhibiting effect of alcohol on the bone healing process, particularly on bone formation and neovascularization, remains insufficiently understood.

MicroRNAs (miRNAs/miRs) are approximately 22-nucleotide noncoding RNAs involved in a variety of biological processes, including tumour progression, metabolic disease development, and stem cell self-renewal and differentiation.[28,29] They can inhibit gene expression at the post-transcriptional level by imperfectly binding to 3'-untranslated regions (3'-UTRs). Several miRNAs play pivotal roles in regulating osteogenic differentiation.[30-34]

Methods

Cell isolation and culture. Human umbilical vein endothelial cells (HUVECs) were cultured in an endothelial cell medium (ECM) (ScienCell, USA). BMSCs were cultured in minimum essential medium α (α-MEM) (Gibco BRL, USA) containing 10% fetal bovine serum (FBS, Gibco BRL) and 100 mg/ml penicillin and streptomycin (Gibco BRL). Cells between passages 4 and 7 were used in the following experiments.

miRNA sequencing. BMSCs were cultured in α-MEM supplemented with 10% FBS, 100 mg/ml penicillin and streptomycin, 0.1 μM dexamethasone (Sigma-Aldrich, USA), 50 μg/mL ascorbic acid (Sigma-Aldrich), and 10 μM β-sodium glycerophosphate (Sigma-Aldrich) for three and seven days. Cells cultured in complete medium were used as controls. Total RNA was extracted using TRIzol reagent (Invitrogen, Thermo Fisher Scientific, USA). Single-end sequencing (36 or 50 bp) was performed using Illumina HiSeq 2500 (Illumina, USA).

miRNA synthesis, transfection, and small interfering RNA transfection. HUVECs and BMSCs were cultured in six-well plates and transfected with the overexpression sequence (miR-19a-3p mimic), inhibition sequence (miR-19a-3p inhibitor), or their respective negative control (NC mimic and NC inhibitor), according to the manufacturer's instructions (Ruibo, China) for 24 hours. A chemically modified miRNA agomir (Ruibo) was used in animal experiments. HUVECs and BMSCs were transfected with forkhead box F2 (FOXF2) small interfering RNA (siRNA) or NC FOXF2 siRNA with additional co-treatment for 48 hours, according to the manufacturer's instructions (Ruibo).

Dual-luciferase reporter assay. The FOXF2 3'-UTR fragment containing the predicted potential has-miR-19a-3p binding site was amplified using polymerase chain reaction (PCR) and subcloned downstream of the luciferase gene of the pMIR-reporter luciferase vector (Promega, USA). Human embryonic kidney 293 T cells were cultured in a 96-well plate and transfected with Lipofectamine 2000 (Thermo Fisher Scientific). Luciferase activity was measured using a dual-luciferase reporter assay system (Promega).

Cell proliferation. The proliferation of BMSCs and HUVECs was detected using Cell Counting Kit-8 (CCK-8) (Dojindo, Japan). Cells at a density of 5×10^3/well were cultured in a 96-well plate. Different concentrations of the treatment were added to the plate. On days 1, 3, and 7, CCK-8 solution was added and the cells were incubated for two hours. The absorbance of each well was measured at 450 nm using a microplate reader (Bio-Rad, USA).

Alizarin red staining. BMSCs were seeded in a 24-well plate and cultured in osteogenic differentiation (OB) medium. After 14 days, the cells were fixed with 4% paraformaldehyde for 30 minutes, washed with phosphate-buffered saline (PBS) three times, and stained with alizarin red working solution (Sigma-Aldrich) for five minutes.
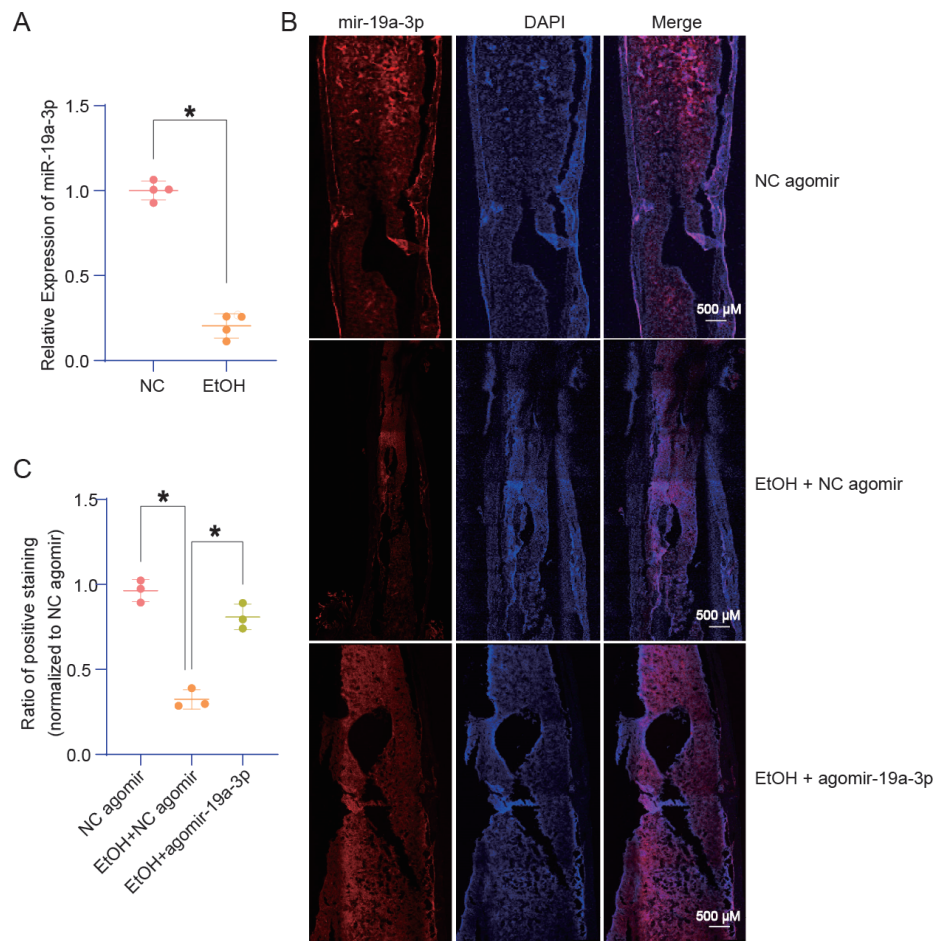
Fig. 1

MicroRNA (miR)-19a-3p is a potential target in alcohol-induced delayed bone fracture healing. a) Expression of miR-19a-3p in femoral bone tissues of ethanol-treated mice compared to control mice. The expression of miR-19a-3p was normalized to U6 (n = 4 femora for each group, p < 0.001, independent-samples t-test). b) Fluorescence in situ hybridization (FISH) staining of miR-19a-3p on bone sections (red). Cell nuclei were visualized using 4′,6-diamidino-2-phenylindole (blue). c) Quantitative results of FISH staining (*p < 0.001, one-way analysis of variance; n = 3). EtOH, ethanol; NC, negative control.

After washing with PBS three times, images were captured with a light microscope.

Alkaline phosphatase activity. BMSCs were seeded in a 24-well plate and cultured in OB medium. After 14 days, the cells were fixed with 4% paraformaldehyde for 30 minutes, washed with PBS three times, and incubated in alkaline phosphatase (ALP) staining buffer according to the manufacturer's instructions (Jiancheng, China). After 30 minutes of incubation, the cells were washed with PBS and imaged under a light microscope. An ALP assay kit was purchased for ALP activity determination. The assay was performed according to the manufacturer's instructions (Jiancheng). The absorbance was measured at 520 nm.

In vitro vascularization assay. HUVECs were seeded in a 96-well plate coated with cold ECM gel (Sigma-Aldrich). Thereafter, the HUVECs were treated with the indicated supplements. Tube formation assay was performed, and the results were examined under a microscope (Leica, Germany) after 12 hours.

HUVECs (3 × 10⁴/well) were cultured in 200 μl basal medium containing 1% FBS. The cells were then seeded into the upper chamber of a transwell plate (Corning, China). The lower chamber was supplemented with basal medium containing 5% FBS and the indicated treatments. After 24 hours, the upper chamber was fixed with 4% paraformaldehyde for 30 minutes, washed with PBS three times, and stained with 0.5% crystal violet (Beyotime, China) for two minutes. Cell migration in the transwell assay was examined using an optical microscope.

HUVECs were cultured in a six-well plate until they reached confluence. A 200 μl sterile loading gun was used to divide the cells to form a cell-free area in the centre of the culture plate. PBS was used to wash the cellular debris three times. Thereafter, the cells were cultured in basal medium containing 1% FBS and the indicated treatment. The scratch wound assay was performed immediately thereafter and 12 hours later, and the results were observed using a microscope.
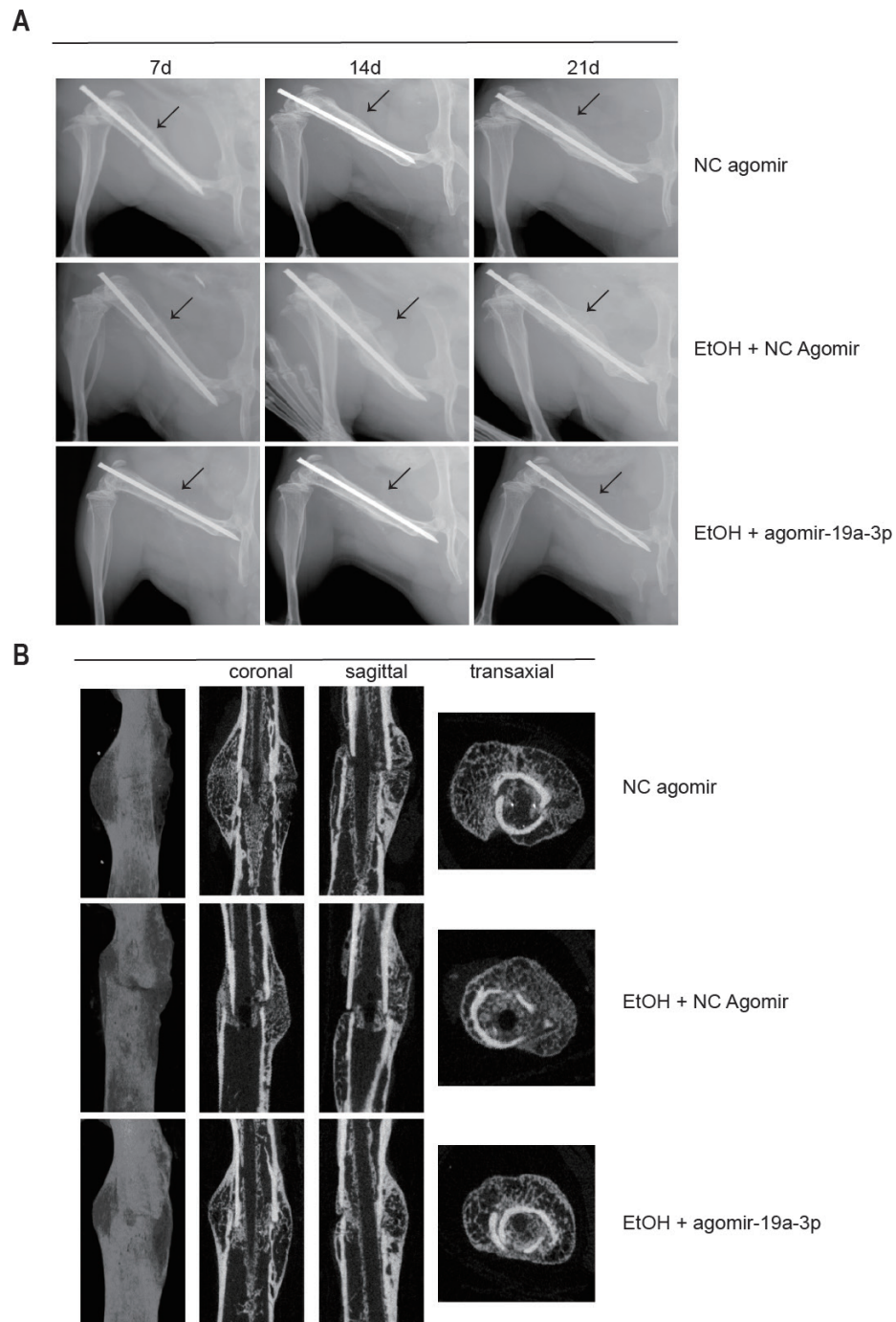
Fig. 2

Alcohol-impaired bone fracture healing is rescued by microRNA (miR)-19a-3p. a) Radiological imaging of femora. b) Micro-CT imaging of femora. EtOH, ethanol; NC, negative control.

Real-time PCR. Total RNA was extracted from BMSCs and HUVECs using the TRIzol Up kit (TransGen Biotech, China). The PCR reaction system was prepared to a total reaction volume of 10 μl with 5 μl 2× PCR buffer, 0.2 μl upstream primers, 0.2 μl downstream primers, 2 μl complementary DNA (cDNA), and 2.6 μl double-distilled water. The reaction conditions were as follows: 95°C for five minutes, 95°C for ten seconds, and 60°C for 30 seconds (a total of 40 cycles).

Western blot. Total proteins were extracted using radio-immunoprecipitation assay buffer containing phosphate and protease inhibitors. Proteins were separated using sodium dodecyl sulfate-polyacrylamide gel electrophoresis
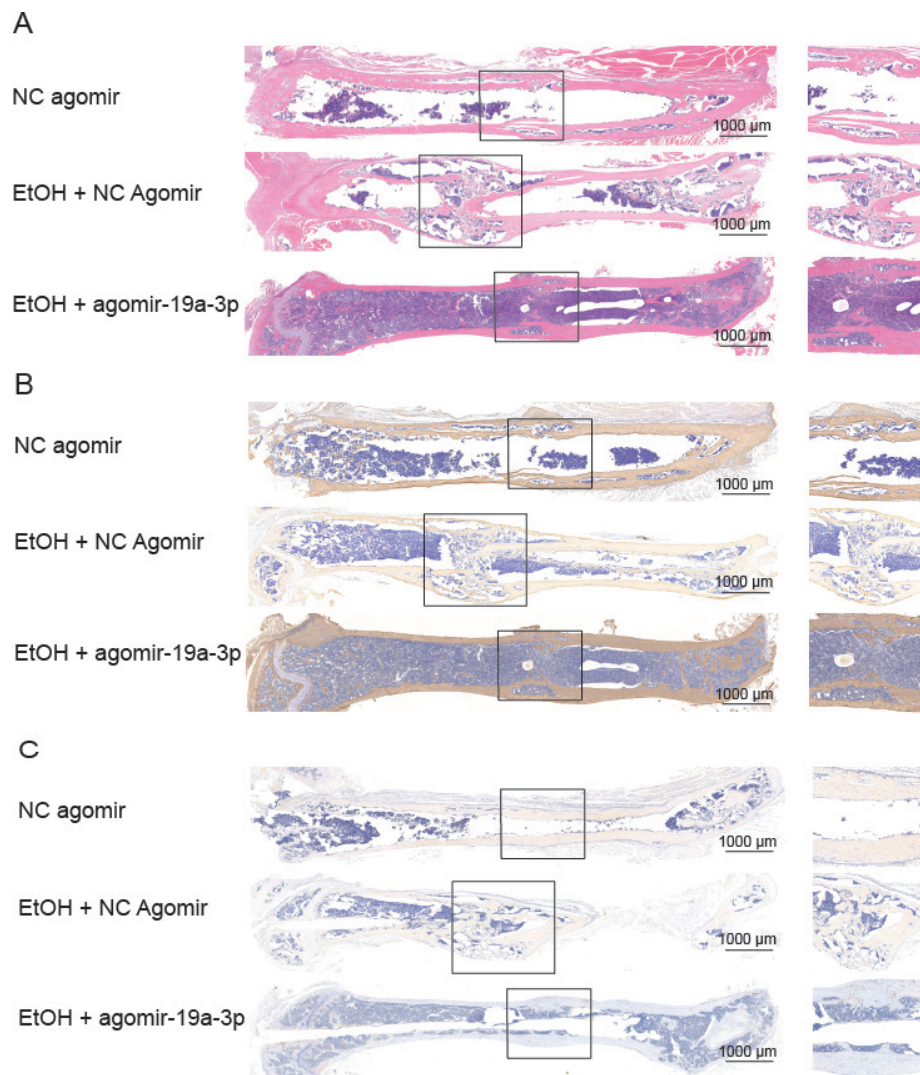
Fig. 3

Inhibition of microRNA (miR)-19a-3p can impair bone regeneration. a) Haematoxylin and eosin staining of fracture sites. b) Immunohistochemical staining with COL-1. c) Immunohistochemical staining with matrix metalloproteinase 13 (MMP13) (left column magnification 20×; right column magnification 60×). EtOH, ethanol; NC, negative control.

and transferred to membranes. FOXF2 and glyceraldehyde 3-phosphate dehydrogenase (GAPDH) antibodies (Cell Signaling Technology, USA) and goat anti-rabbit IgG secondary antibody (Cell Signaling Technology) were purchased. An electrogenerated chemiluminescence developer solution (Millipore, USA) was used to detect the bands.

Animal grouping and treatment. This study conformed to the Animal Research: Reporting of In Vivo Experiments (ARRIVE) guidelines, and an ARRIVE checklist was completed and is included in the Supplementary Material. The sample size was calculated on the basis of a pilot study. A total of 60 male C57BL/6 mice were used. The mice were randomly divided into the following groups: 1) control (NC agomir), 2) ethanol (EtOH+ NC agomir), and 3) ethanol and agomir-19a-3p (EtOH+ agomir-19a-3p) groups. Mice in the EtOH+ NC agomir and EtOH+

agomir-19a-3p groups were fed with water containing 10% ethanol for three weeks, as previously described.[35] The mice were placed under anaesthesia. A small incision was made near the anterior distal femur, after shaving the fur. A 25-gauge needle was inserted through the intramedullary canal to the sub- or intertrochanteric femur. Subsequently, a mid-shaft fracture was generated, as previously described.[3] The cuts were closed layer-by-layer using 5-0 silk sutures. Mice in the EtOH+ NC agomir and EtOH+ agomir-19a-3p groups were continuously fed with water containing 10% ethanol. The animals were killed, and fractured femora were harvested for the subsequent tests. To minimize potential confounders, all animals received daily treatments simultaneously. No infections or other complications were observed in any of the animals. All mice were included in the data analysis.
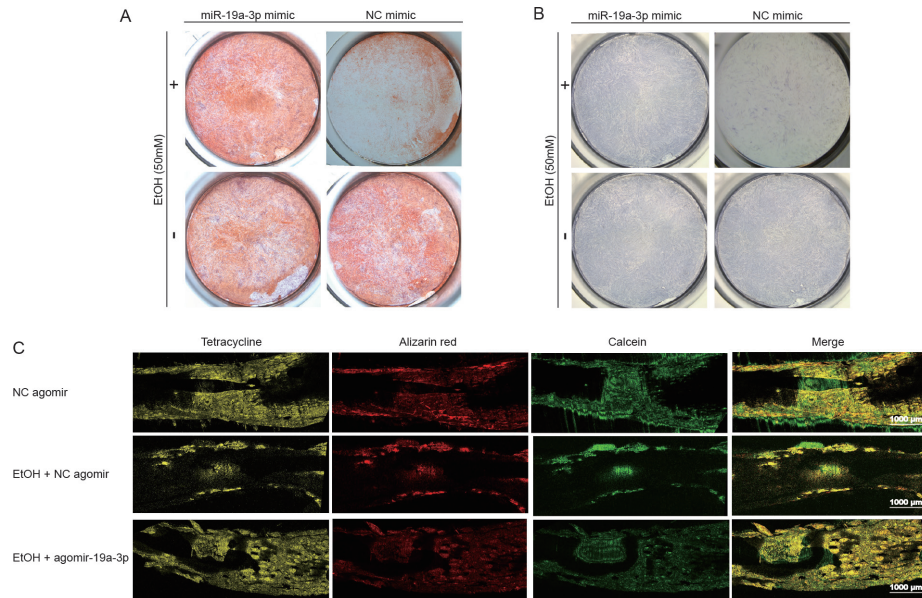
Fig. 4

MicroRNA (miR)-19a-3p can alleviate the impaired osteogenic differentiation caused by ethanol (EtOH). a) Alizarin red staining of bone mesenchymal stem cells (BMSCs) incubated in osteogenic differentiation (OB) medium containing the indicated treatments for 14 days (magnification 2×). b) Alkaline phosphatase (ALP) staining of BMSCs incubated in OB medium containing the indicated treatments for 14 days (magnification 2×). c) Fluorochrome labelling of the fracture site. Tetracycline, alizarin red, and calcein produced yellow, red, and green staining, respectively. NC, negative control.

Biomechanical testing. A three-point bending test was performed using an axial servohydraulic testing system with a 100 N load cell.[36] The femoral callus was positioned at the centre, and a central load was applied at a rate of 0.05 mm/s. Load deflection curves were plotted to determine the maximum load. Intact femora from seven untreated male C57BL/6 mice were used as blank controls.

Radiological and micro-CT imaging. Plain radiological images of the femora were obtained at seven, 14, and 21 days post-surgery. Image analysis was performed using the common format (DICOM). Micro-CT was performed with a micro-CT scanner (Skyscan 1176; Bruker, Belgium) set at a 9 μm voxel size. The images were processed and reconstructed using the CTVol software (Bruker), as previously described. The trabecular bone volume fraction (BV/TV), relative callus volume, trabecular spacing (Tb.Sp), and bone mineral density (BMD) were measured from the reconstructed images.

Histological and immohistochemical analyses. Bone specimens were decalcified with 10% ethylenediaminetetraacetic acid for 14 days. The bone tissue was then embedded in paraffin and cut into 5-μm-thick sections. Haematoxylin and eosin (H&E) staining, safranin-fixed green staining, and Masson's trichrome staining were performed. A Leica DM4000 microscope (Leica) was used to capture images. Immunofluorescence staining was performed on frozen sections, and images were acquired using an SP8 confocal microscope (Leica). Anti-CD31, collagen-1 (COL-1), and matrix metalloproteinase 13 (MMP13) antibodies were obtained from Abcam (China). Fluorescence in situ hybridization (FISH) was performed

on frozen sections, and images were acquired using an SP8 confocal microscope (Leica). The probe of miR-19a-3p was obtained from Ruibo.

To observe dynamic bone formation, tetracycline (25 mg/kg; Aladdin, China), alizarin red (30 mg/kg, Aladdin), and calcein AM (10 mg/kg, Aladdin) were injected intramuscularly at one, two, and three weeks post-surgery. After the animal kill and specimen preparation, bone formation was observed using a confocal laser-scanning microscope (Leica).

Statistical analysis. All data are expressed as mean and standard deviation from at least three individual repeated experiments. Statistical analysis was performed using SPSS 20.0 (IBM, USA). An independent-samples t-test was used to examine significant differences between two groups, and one-way analysis of variance was used to examine significant differences in multiple comparisons. Statistical significance was set at $p < 0.05$.

Results

miR-19a-3p is a potential target in alcohol-inhibited bone fracture healing. miRNAs play pivotal roles in the different stages of osteogenesis and fracture healing.[29,37,38] BMSCs are the basic cell unit of embryonic bone formation. These cells have been widely used in regenerative medicine because of their unique capabilities of self-renewal and multilineage differentiation.[39,40] The formation of vessels can facilitate bone regeneration, which can be evaluated using HUVECs. To identify the key miRNAs in fracture healing, BMSCs were used as target cells for miRNA scanning; miRNA sequencing was performed on
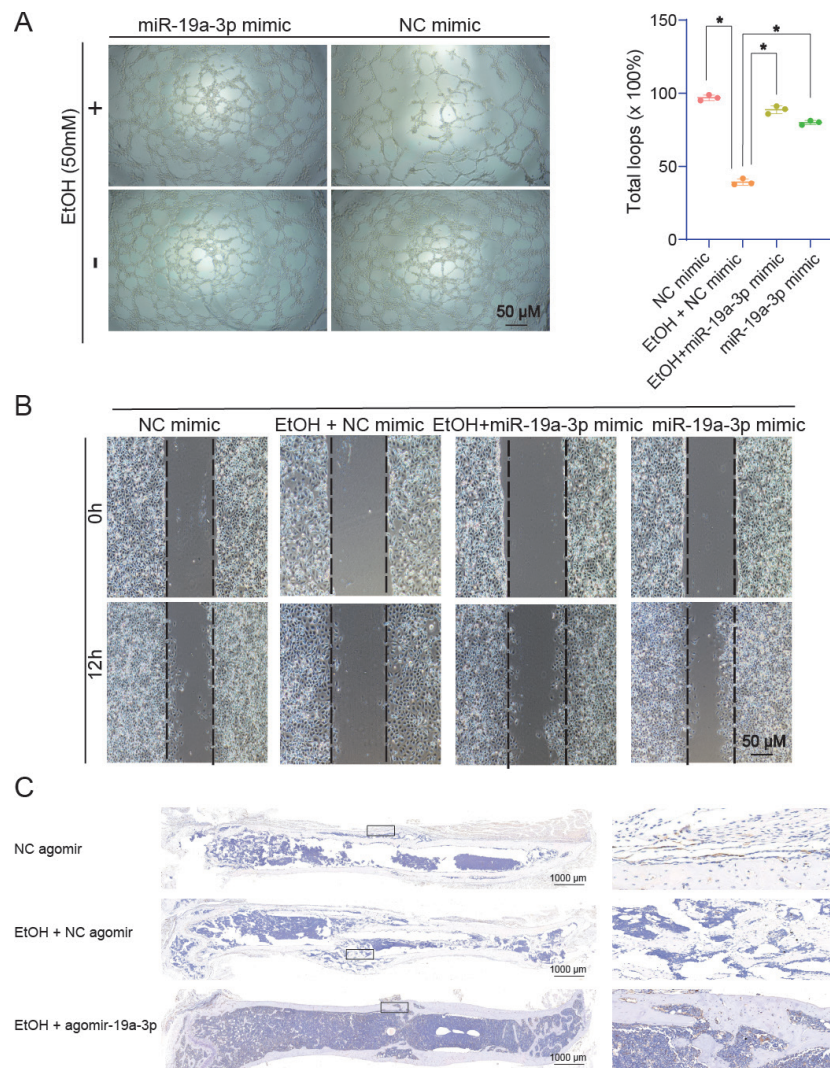
Fig. 5

MicroRNA (miR)-19a-3p benefits alcohol-impaired vascularization both in vitro and in vivo. a) Tube formation by human umbilical vein endothelial cells (HUVECs) incubated with the indicated treatments for 12 hours in Matrigel. b) Scratch wound assay for measuring cell migration. c) CD31 staining of the fracture sites (n = 3 for each group, *p < 0.001, one-way analysis of variance) (left column magnification 20×; right column magnification 60×). EtOH, ethanol; NC, negative control.

BMSCs treated with osteogenic differentiation medium for three and seven days. Among the differentially expressed miRNAs, 27 were selected because of significant changes across three timepoints (Supplementary Figure aa). Overall, 15 of these differential miRNAs were further validated according to whether ethanol can regulate their expression. BMSCs were treated with 50 mM ethanol for three days, and RT-PCR was performed (Supplementary Figure ab). miR-19a-3p was upregulated during osteogenesis but was downregulated by ethanol; among the differentially expressed miRNAs, only four were significantly downregulated by ethanol (miR-129-5 p, miR-133a-3p, miR-6842-3 p, and miR-19a-3p). BMSCs treated with these four miRNAs were stained with alizarin red. Only miR-19a-3p reversed the inhibitory effects of ethanol on osteogenic differentiation. The miR-19a-3p expression in the bones of ethanol-treated mice was significantly lower than that in the bones of normal control mice (Figure 1a). Therefore, in this study, miR-19a-3p was selected as the target miRNA of interest in the pathogenesis of alcohol-impaired fracture healing.

We established an alcohol-fed mouse model to observe the process of fracture healing. FISH was performed to evaluate the expression of miR-19a-3p in the fracture sites of mice. As shown in Figure 1b, positive staining for miR-19a-3p was observed in the NC agomir group. In the EtOH+ NC agomir group, the positive staining was significantly decreased. Administration of agomir-19a-3p promoted the expression of miR-19a-3p. The quantitative results are shown in Figure 1c.

Alcohol-induced delayed bone fracture healing is rescued by miR-19a-3p. Supplementary Figure b shows a schematic of the experimental design. Biomechanical testing has been widely adopted in assessing the quality of
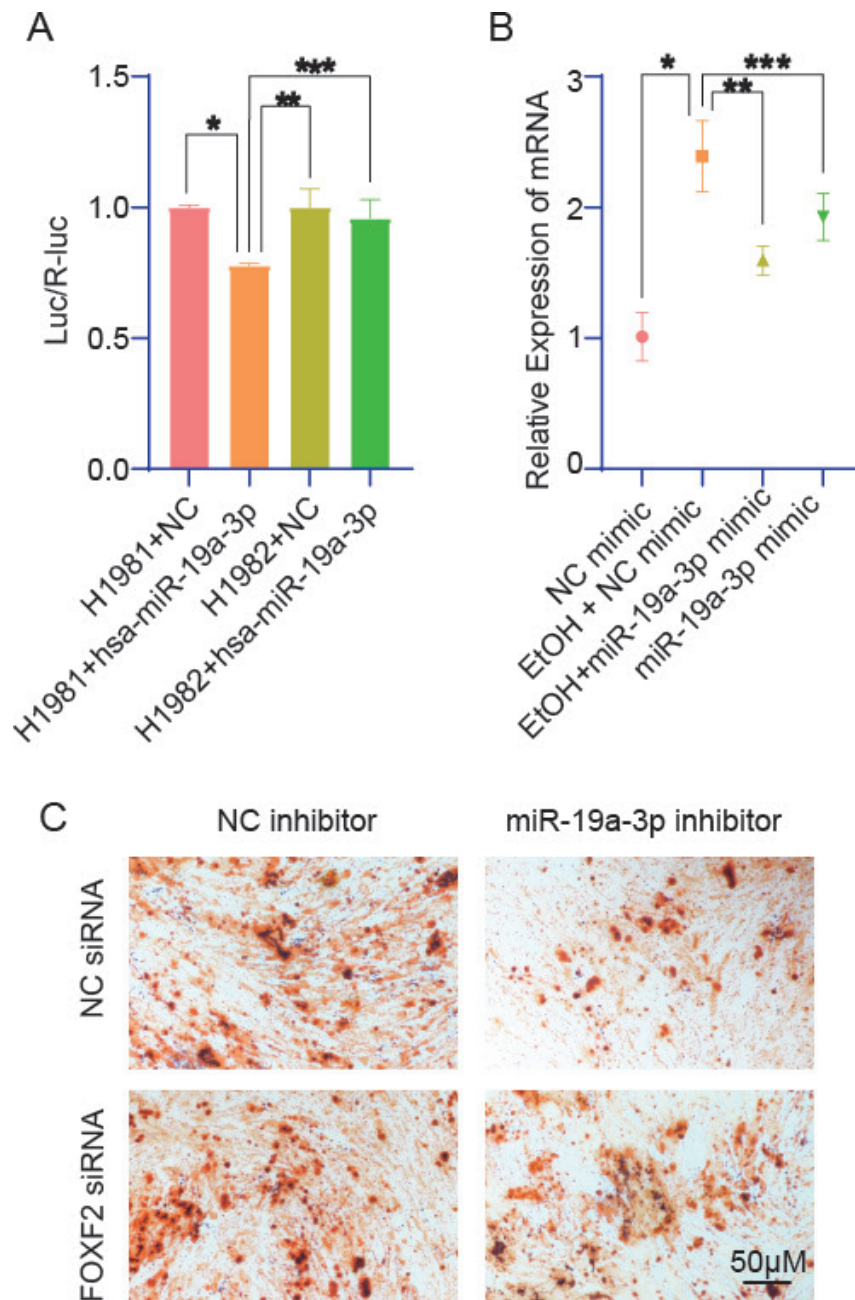
Fig. 6

Forkhead box F2 (FOXF2) is the direct downstream target of microRNA (miR)-19a-3p. a) Luciferase reporter genes, including a wild type FOXF2 3′-untranslated region (3′-UTR) and a FOXF2 3′-UTR containing mutant sequences of the miR-19a-3p binding site, were generated in 293 T cells (*p < 0.001, **p = 0.006, ***p = 0.011). b) The messenger RNA expression of FOXF2 in bone mesenchymal stem cells (BMSCs) was measured using real-time polymerase chain reaction after the indicated treatment (*p = 0.002, **p = 0.009, ***p = 0.069). c) Alizarin red staining of BMSCs incubated in OB medium containing the indicated treatments for 14 days (n = 3 for each group, one-way analysis of variance). siRNA, small interfering RNA.

fracture healing.[41,42] As shown in Supplementary Figures ca to cb and Figure 2, both the binding rigidity and modulus of elasticity (E-modulus) were decreased after fracture compared to the untreated group. The administration of ethanol significantly reduced the biomechanical strength (p < 0.05, one-way analysis of variance). These effects were abolished by treatment with agomir-19a-3p. To observe dynamic bone healing, radiological imaging was conducted at seven, 14, and 21 days post-surgery. Mice in the NC agomir and EtOH+ agomir-19a-3p groups had almost achieved fracture union at 21 days. However, in the EtOH+ NC agomir group, fracture healing was not complete at 21 days, with a hypertrophic callus remnant. In addition, more calluses appeared in the EtOH+ NC agomir group at 14 and 21 days than in the NC agomir and EtOH+ agomir-19a-3p groups (Figure 2a). Femora were

harvested and evaluated using micro-CT at 28 days post-surgery (Figure 2b). The BV/TV, Tb.Sp, and BMD were decreased in the EtOH+ NC agomir group, and these effects were reversed by miR-19a-3p treatment (Supplementary Figure d). The results of H&E staining showed that the bone fracture healed well, with few calluses remaining in the NC agomir and EtOH+ agomir-19a-3p groups (Figure 3a). However, abundant callus surrounded the fracture sites in the EtOH+ NC agomir group. Masson's trichrome staining showed similar trends (Supplementary Figure ea). Safranin-fixed green staining showed that the calluses in the ethanol group mainly consisted of cartilage (Supplementary Figure eb). As shown in Figure 3b and Supplementary Figure fa, the positive staining for COL-1 was reduced in the EtOH+ NC agomir group compared to the NC agomir and EtOH+ agomir-19a-3p groups. MMP13 is a marker of chondrocyte hypertrophic differentiation;[43] positive staining for MMP13 was abundantly observed in the NC agomir and EtOH+ NC agomir groups, whereas it was rare in the EtOH+ agomir-19a-3p group (Figure 3c and Supplementary Figure fb). These interesting findings indicate that the inhibitory effect of ethanol on fracture healing may be ascribed to the suppression of hypertrophic chondrocyte transdifferentiation and, in part, apoptosis.[44]

miR-19a-3p overexpression reverses alcohol-impaired bone formation. We examined the effects of miR-19a-3p on the osteogenic differentiation of BMSCs. The CCK-8 results indicated that miR-19a-3p had no inhibitory or promotional effect on the proliferation of BMSCs (Supplementary Figure g). Alizarin red staining demonstrated that ethanol inhibited the osteogenic differentiation of BMSCs, but miR-19a-3p reversed these inhibitory effects (Figure 4a). The direct use of miR-19a-3p did not alter the osteogenic differentiation of BMSCs compared to that in the control group. The ALP staining results showed similar trends (Figure 4b and Supplementary Figure ha). The results of RT-PCR showed that ethanol decreased the expression of COL-1, OCN, and ALP in BMSCs, and miR-19a-3p alleviated this effect (Supplementary Figures hb to hd). The results of western blotting showed that the protein levels of RUNX2, COL-1, OCN, and ALP were downregulated by ethanol and upregulated by miR-19a-3p (Supplementary Figure i). These data collectively demonstrated that the inhibited osteogenic differentiation of ethanol-treated BMSCs in vitro was partially rescued by miR-19a-3p overexpression. As shown in Figure 4c, numerous areas positive for tetracycline (yellow), alizarin red (red), and calcein (green) staining were observed in the NC agomir group. Ethanol significantly reduced the positive staining. After the administration of agomir-19a-3p, more dynamic bone formation was observed.

miR-19a-3p benefits alcohol-impaired vascularization both in vitro and in vivo. Optimal bone repair necessitates the coordinated regeneration of osseous and vascular structures. The maturation of soft calluses into hard calluses relies on the invasion of new blood vessels. Therefore,

the effects of miR-19a-3p and ethanol on vascularization were further investigated. The CCK-8 results indicated that miR-19a-3p had no inhibitory or promotional effect on the proliferation of BMSCs (Supplementary Figure j). Tube formation by HUVECs was significantly suppressed by ethanol, whereas miR-19a-3p alleviated this effect (Figure 5a) (p < 0.001, one-way analysis of variance). Scratch wound and transwell assays were used to evaluate cell migration. As shown in Figure 5b and Supplementary Figure k, ethanol inhibited the migration of HUVECs. Meanwhile, miR-19a-3p increased the number of migrated HUVECs. The quantitative results of the transwell assay are shown in Supplementary Figure l. The results were in accordance with the scratch wound assay results. The RT-PCR results indicated that the messenger RNA (mRNA) level of VEGF was decreased by ethanol and recovered by miR-19a-3p (Supplementary Figure m). The results of CD31 staining of the fracture sites are shown in Figure 5c. More positive staining was observed in the NC agomir and EtOH+ agomir-19a-3p groups, whereas only a few positive staining areas were observed in the EtOH+ NC agomir group. The quantitative results are presented in Figure 5 and Supplementary Figure n. These observations indicate less blood vessel formation in the EtOH+ NC agomir group, which may be attributed to the suppression of vascularization in endothelial cells. Insufficient new vascular formation hindered the maturation of hypertrophic chondrocytes, which eventually led to delayed fracture healing.

FOXF2 is the direct downstream target of miR-19a-3p. To further investigate the underlying mechanism, online biological prediction software was used to predict the target of miR-19a-3p.[45] Only miRNAs conserved among the different species that target conserved gene transcripts were analyzed. As shown in Figure 6 and Supplementary Figure o, we predicted that FOXF2 is the target site of miR-19a-3p. To test whether miR-19a-3p directly targets FOXF2, luciferase reporter genes, including a wild-type (WT) FOXF2 3′-UTR and a FOXF2 3′-UTR containing mutant sequences of the miR-19a-3p binding site (Mut), were generated in 293 T cells. The WT or Mut luciferase reporter was cotransfected with miR-19a-3p or the NC mimic. The luciferase reporter activity of WT FOXF2 3′-UTR was inhibited by miR-19a-3p. However, miR-19a-3p only slightly inhibited the luciferase reporter activity of Mut FOXF2 3′-UTR (Figure 6a).

To further investigate the underlying mechanism of the effect of miR-19a-3p on ethanol-associated delayed bone formation, specific siRNA and miRNA inhibitors were administered to knock down the expression of FOXF2 and miR-19a-3p. The protein level of FOXF2 was increased in BMSCs treated with ethanol. Transfection with miR-19a-3p antagonized the elevation of FOXF2 levels (Figure 6b and Supplementary Figure p). Alizarin red staining showed that FOXF2 silencing recovered the osteogenic differentiation inhibited by the miR-19a-3p inhibitor (Figure 6c). The RT-PCR results showed similar trends (Supplementary Figure q). Taken together, the

inhibitory effect of ethanol on osteogenesis may be associated with the miR-19a-3p/FOXF2 axis.

Discussion

Zhu et al[46] demonstrated that ethanol can impair bone formation and vascularization in osteonecrosis of the femoral head. Ethanol regulates the miR-136-3p/PTEN axis in vascularization and bone formation, which can lead to osteopenia. In this study, we showed that alcohol had a deleterious effect on fracture repair in mice. We found that miR-19a-3p modulates the expression of FOXF2 to regulate bone formation and vascularization during fracture healing. Therefore, miR-19a-3p is a potential therapeutic target in alcohol-impaired fracture healing.

Chronic and heavy alcohol consumption is a well-recognized risk factor for osteoporosis and bone fracture.[47–49] Numerous clinical studies have demonstrated an association between alcohol intake and an increased risk of fracture nonunion and delayed union.[13] Therefore, there is an urgent need to elucidate the specific mechanisms involved. Adequate blood supply is one of the crucial factors influencing the bone fracture healing process. Coupled vascularization and osteogenesis is crucial for maintaining bone homeostasis; the defining feature of nonunion is impaired vascularization.[50,51] Thus, a strategy to enhance osteogenesis and vascularization is urgently needed. HUVECs are endothelial cells frequently used in evaluating angiogenesis.[52] In vitro studies have shown that miR-19a-3p can promote the migration, tube formation ability, and VEGF expression of HUVECs. The results of CD31 staining in our study (Figure 3) also showed that miR-19a-3p can enhance the vascularization of fracture sites. Hypertrophic chondrocytes are the master regulators of endochondral ossification. The receptor activator of nuclear factor kappa-B ligand expressed in hypertrophic chondrocytes induces osteoclastogenesis and maintains the balance between bone resorption and formation.[53] Hypertrophic chondrocytes also express VEGF, which can induce angiogenesis and vascularization of the ossification centre.[54] We found less positive staining for MMP13 in the EtOH+ NC agomir group, which was in parallel with a decrease in CD31 and vascular ingrowth. However, a significantly higher volume of callus formation was observed in the EtOH+ NC agomir group than in the NC agomir group (p < 0.001, one-way analysis of variance). These seemingly contradictory results can be attributed to the detrimental effects of alcohol on the maturation of bone callus, which impairs the transformation of hypertrophic chondrocytes and the process of neovascularization. Previous studies reported that alcohol consumption decreased the callus volume formed in a mammalian model of femoral fracture. This may be due to the difference in the alcohol application methods in animal models. Interestingly, some bone and cartilage formation was observed in the EtOH+ NC agomir group. The volume of callus in the EtOH+ NC agomir group was higher than that in the NC agomir group, in which the callus mainly consisted of hypertrophic chondrocytes. This might have contributed to the lack of newly formed vessels and the subsequent immaturity of hypertrophic chondrocytes.

Multiple miRNAs have been demonstrated to be involved in osteogenic differentiation by regulating related signalling pathways.[32–34,38,55] However, only a few studies have focused on the role of miRNAs in the regulation of ethanol-influenced bone formation. To investigate the role of miRNAs in these processes, we performed miRNA sequencing analysis of BMSCs and bioinformatics analysis. Among the differentially expressed miRNAs, miR-19a-3p alleviated the ethanol-associated impairment of bone formation and vascularization. FISH staining showed that the expression of miR-19a-3p in the fracture sites was downregulated by ethanol. miR-19a-3p is a member of the miR-17-92 cluster, which is involved in the proliferation, apoptosis, and metastasis of different malignant tumours.[56–59] The miR-19a-3p inhibitor can increase the expression of p53, Bax, and caspase-3, and decrease the expression of Bcl-2.[60] In our study, we observed that miR-19a-3p recovered the osteogenic differentiation and vascularization capacity impaired by ethanol. In the mouse model of femur fracture, agomir-19a-3p promoted fracture healing, which was inhibited by ethanol. Previous studies have demonstrated that alcoholic liver cirrhosis was associated with lower measures of bone strength (e.g. lower areal BMD, cross-sectional area, and section modulus; thinner cortex; and higher buckling ratio).[61] We also checked for liver damage. However, H&E staining revealed no significant pathological abnormalities. This may be attributed to the intermediate dosage and the timing of our treatment.[62] H&E staining of the heart, spleen, lungs, and kidneys was performed, and no obvious changes were observed in these tissues. As miR-19a-3p was selected from the miRNA sequencing performed on BMSCs, which are the basic cell unit of embryonic bone formation, the results of our study are specific to bone tissue. The osteogenic differentiation of BMSCs can be directly inhibited by ethanol, whereas it can be rescued by miR-19a-3p. Meanwhile, miR-19a-3p promotes ethanol-delayed fracture union through the enhancement of angiogenesis, which is an indirect effect. Taken together, miR-19a-3p reverses the ethanol-induced delay in fracture union both directly and indirectly.

FOXF2 is a homeobox protein that maintains tissue homeostasis. It can promote the differentiation of mesenchymal cells and inhibit the mesenchymal transformation of adjacent epithelial cells. The regulation of FOXF2 can influence the tumorigenesis, progression, and metastasis of breast cancer and other cancer types.[63–65] In this study, FOXF2 was found to be the downstream target of miR-19a-3p. The regulation of FOXF2 can influence the effect of miR-19a-3p on osteogenic differentiation.

Long-term excessive alcohol drinking has long-lasting effects on the bone. A decrease in BMD has been observed at different skeletal sites, including the forearm, spine, iliac crest, and trochanter, in individuals with an alcohol consumption of between 100 and 200 g/day for

many years.[66] Previous studies have shown that individuals who suffer from alcoholism experience significantly longer bone fracture healing times than those who do not.[67] In our study, we fed mice with alcohol both before and after surgery, and we mainly focused on the effects of binge alcohol exposure on fracture union. The results showed that binge alcohol exposure can delay fracture union in mice. In individuals with chronic heavy alcohol consumption, abstinence for six months was associated with an increase in bone mass, osteocalcin, and serum vitamin D levels.[66] A rapid increase in osteocalcin after two weeks of withdrawal was reported by Pepersack et al.[68] In addition, Nyquist et al[69] found that animals that received alcohol before fracture and were placed in abstinence after injury had normal biomechanical properties of the fracture callus. Considering the deleterious effects of alcohol on the bone, patients should be advised to stop alcohol consumption. In patients with fracture, stopping alcohol consumption after the injury would facilitate fracture healing.

In conclusion, ethanol can decrease the expression of miR-19a-3p, which contributes to elevated levels of FOXF2. As a result, bone formation and vascularization both become impaired and cooperatively delay the healing of bone fractures in mice (Supplementary Figure r). Previous studies have mainly focused on the relationship between chronic heavy alcohol consumption and fracture union.[10,11] The results of this study showed that excessive alcohol consumption can contribute to the failure of fracture healing, whereas miR-19a-3p can reverse this effect. Further studies should focus on the changes in miR-19a-3p levels in the bone tissues of patients with traumatic fractures who are heavy drinkers. The miR-19a-3p/FOXF2 axis serves as the foundation of alcohol-impaired fracture healing and may be a potential therapeutic target.

Supplementary material

The differential microRNAs, biomechanical testing, quantification of staining, other detailed experimental data, graphic abstract, and ARRIVE checklist.

References

1. **Claes L**, **Recknagel S**, **Ignatius A**. Fracture healing under healthy and inflammatory conditions. *Nat Rev Rheumatol*. 2012;8(3):133–143.
2. **Einhorn TA**, **Gerstenfeld LC**. Fracture healing: mechanisms and interventions. *Nat Rev Rheumatol*. 2015;11(1):45–54.
3. **Einhorn TA**. Enhancement of fracture-healing. *J Bone Joint Surg Am*. 1995;77-A(6):940–956.
4. **Zura R**, **Xiong Z**, **Einhorn T**, **et al**. Epidemiology of fracture nonunion in 18 human bones. *JAMA Surg*. 2016;151(11):e162775.
5. **Walter N**, **Rupp M**, **Hierl K**, **et al**. Long-term patient-related quality of life after fracture-related infections of the long bones. *Bone Joint Res*. 2021;10(5):321–327.
6. **Chang C-J**, **Jou I-M**, **Wu T-T**, **Su F-C**, **Tai T-W**. Cigarette smoke inhalation impairs angiogenesis in early bone healing processes and delays fracture union. *Bone Joint Res*. 2020;9(3):99–107.
7. **Nicholson T**, **Scott A**, **Newton Ede M**, **Jones SW**. Do E-cigarettes and vaping have a lower risk of osteoporosis, nonunion, and infection than tobacco smoking? *Bone Joint Res*. 2021;10(3):188–191.
8. **Komatsu DE**, **Warden SJ**. The control of fracture healing and its therapeutic targeting: improving upon nature. *J Cell Biochem*. 2010;109(2):302–311.
9. **Cheng C**, **Shoback D**. Mechanisms underlying normal fracture healing and risk factors for delayed healing. *Curr Osteoporos Rep*. 2019;17(1):36–47.
10. **Berg KM**, **Kunins HV**, **Jackson JL**, **et al**. Association between alcohol consumption and both osteoporotic fracture and bone density. *Am J Med*. 2008;121(5):406–418.
11. **Kanis JA**, **Johansson H**, **Johnell O**, **et al**. Alcohol intake as a risk factor for fracture. *Osteoporos Int*. 2005;16(7):737–742.
12. **Duckworth AD**, **Bennet SJ**, **Aderinto J**, **Keating JF**. Fixation of intracapsular fractures of the femoral neck in young patients: risk factors for failure. *J Bone Joint Surg Br*. 2011;93-B(6):811–816.
13. **Nicholson JA**, **Makaram N**, **Simpson A**, **et al**. Fracture nonunion in long bones: A literature review of risk factors and surgical management. *Injury*. 2021;52(Suppl 2):S3–S11.
14. **Trevisiol CH**, **Turner RT**, **Pfaff JE**, **et al**. Impaired osteoinduction in a rat model for chronic alcohol abuse. *Bone*. 2007;41(2):175–180.
15. **Chakkalakal DA**, **Novak JR**, **Fritz ED**, **et al**. Inhibition of bone repair in a rat model for chronic and excessive alcohol consumption. *Alcohol*. 2005;36(3):201–214.
16. **Kelly KN**, **Kelly C**. Pattern and cause of fractures in patients who abuse alcohol: what should we do about it? *Postgrad Med J*. 2013;89(1056):578–583.
17. **Stewart S**, **Darwood A**, **Masouros S**, **Higgins C**, **Ramasamy A**. Mechanotransduction in osteogenesis. *Bone Joint Res*. 2020;9(1):1–14.
18. **Chow S-H**, **Chim Y-N**, **Wang J-Y**, **Wong R-Y**, **Choy V-H**, **Cheung W-H**. Inflammatory response in postmenopausal osteoporotic fracture healing. *Bone Joint Res*. 2020;9(7):368–385.
19. **Wong RMY**, **Choy VMH**, **Li J**, **et al**. Fibrinolysis as a target to enhance osteoporotic fracture healing by vibration therapy in a metaphyseal fracture model. *Bone Joint Res*. 2021;10(1):41–50.
20. **Einhorn TA**. The science of fracture healing. *J Orthop Trauma*. 2005;19(10 Suppl):S4-6.
21. **Nicholson JA**, **Oliver WM**, **MacGillivray TJ**, **Robinson CM**, **Simpson A**. 3D ultrasound reconstruction of sonographic callus: a novel imaging modality for early evaluation of fracture healing. *Bone Joint Res*. 2021;10(12):759–766.
22. **Nicholson JA**, **Oliver WM**, **MacGillivray TJ**, **Robinson CM**, **Simpson A**. Sonographic bridging callus at six weeks following displaced midshaft clavicle fracture can accurately predict healing. *Bone Joint Res*. 2021;10(2):113–121.
23. **Oryan A**, **Monazzah S**, **Bigham-Sadegh A**. Bone injury and fracture healing biology. *Biomed Environ Sci*. 2015;28(1):57–71.
24. **Pountos I**, **Panteli M**, **Panagiotopoulos E**, **Jones E**, **Giannoudis PV**. Can we enhance fracture vascularity: What is the evidence? *Injury*. 2014;45 Suppl 2:S49-57.
25. **Chen Y**, **Yu H**, **Zhu D**, **et al**. miR-136-3p targets PTEN to regulate vascularization and bone formation and ameliorates alcohol-induced osteopenia. *FASEB J*. 2020;34(4):5348–5362.
26. **Léger C**, **Dupré N**, **Laquerrière A**, **et al**. In utero alcohol exposure exacerbates endothelial protease activity from pial microvessels and impairs GABA interneuron positioning. *Neurobiol Dis*. 2020;145:105074.
27. **Di Rocco G**, **Baldari S**, **Pani G**, **Toietta G**. Stem cells under the influence of alcohol: effects of ethanol consumption on stem/progenitor cells. *Cell Mol Life Sci*. 2019;76(2):231–244.
28. **Bartel DP**. MicroRNAs: genomics, biogenesis, mechanism, and function. *Cell*. 2004;116(2):281–297.
29. **Groven RVM**, **van Koll J**, **Poeze M**, **Blokhuis TJ**, **van Griensven M**. miRNAs related to different processes of fracture healing: an integrative overview. *Front Surg*. 2021;8:786564.
30. **Yu H**, **Zhang J**, **Liu X**, **Li Y**, **et al**. microRNA-136-5p from bone marrow mesenchymal stem cell-derived exosomes facilitates fracture healing by targeting LRP4 to activate the Wnt/β-catenin pathway. *Bone Joint Res*. 2021;10(12):744–758.
31. **Liu L**, **Li Z**, **Chen S**, **et al**. *BRD4* promotes heterotopic ossification through upregulation of LncRNA MANCR. *Bone Joint Res*. 2021;10(10):668–676.
32. **Huang J**, **Zhao L**, **Xing L**, **Chen D**. MicroRNA-204 regulates Runx2 protein expression and mesenchymal progenitor cell differentiation. *Stem Cells*. 2010;28(2):357–364.
33. **Kim YJ**, **Bae SW**, **Yu SS**, **Bae YC**, **Jung JS**. miR-196a regulates proliferation and osteogenic differentiation in mesenchymal stem cells derived from human adipose tissue. *J Bone Miner Res*. 2009;24(5):816–825.
34. **Hassan MQ**, **Maeda Y**, **Taipaleenmaki H**, **et al**. miR-218 directs a Wnt signaling circuit to promote differentiation of osteoblasts and osteomimicry of metastatic cancer cells. *J Biol Chem*. 2012;287(50):42084–42092.
35. **Shimizu Y**, **Sakai A**, **Menuki K**, **et al**. Reduced bone formation in alcohol-induced osteopenia is associated with elevated p21 expression in bone marrow cells in aldehyde dehydrogenase 2-disrupted mice. *Bone*. 2011;48(5):1075–1086.

36. **O'Neill KR**, **Stutz CM**, **Mignemi NA**, **et al**. Micro-computed tomography assessment of the progression of fracture healing in mice. *Bone*. 2012;50(6):1357–1367.

37. **Osagie-Clouard L**, **Meeson R**, **Sanghani-Kerai A**, **Bostrom M**, **Briggs T**, **Blunn G**. The role of intermittent PTH administration in conjunction with allogenic stem cell treatment to stimulate fracture healing. *Bone Joint Res*. 2021;10(10):659–667.

38. **Inose H**, **Ochi H**, **Kimura A**, **et al**. A microRNA regulatory mechanism of osteoblast differentiation. *Proc Natl Acad Sci U S A*. 2009;106(49):20794–20799.

39. **De Keyser J**. Autologous mesenchymal stem cell transplantation in stroke patients. *Ann Neurol*. 2005;58(4):653–654.

40. **Tang YL**, **Zhao Q**, **Zhang YC**, **et al**. Autologous mesenchymal stem cell transplantation induce VEGF and neovascularization in ischemic myocardium. *Regul Pept*. 2004;117(1):3–10.

41. **Lauing KL**, **Roper PM**, **Nauer RK**, **Callaci JJ**. Acute alcohol exposure impairs fracture healing and deregulates β-catenin signaling in the fracture callus. *Alcohol Clin Exp Res*. 2012;36(12):2095–2103.

42. **Sun Y**, **Xu L**, **Huang S**, **et al**. mir-21 overexpressing mesenchymal stem cells accelerate fracture healing in a rat closed femur fracture model. *Biomed Res Int*. 2015;2015:412327.

43. **Bertrand J**, **Kräft T**, **Gronau T**, **et al**. BCP crystals promote chondrocyte hypertrophic differentiation in OA cartilage by sequestering Wnt3a. *Ann Rheum Dis*. 2020;79(7):975–984.

44. **van der Stok J**, **Koolen MKE**, **Jahr H**, **et al**. Chondrogenically differentiated mesenchymal stromal cell pellets stimulate endochondral bone regeneration in critical-sized bone defects. *Eur Cell Mater*. 2014;27:137–148.

45. **No authors listed**. Search for predicted microRNA targets in mammals. Whitehead Institute for Biomedical Research. 2021. http://www.targetscan.org/ (date last accessed 25 May 2022).

46. **Zhu D**, **Yu H**, **Liu P**, **et al**. Calycosin modulates inflammation via suppressing TLR4/NF-κB pathway and promotes bone formation to ameliorate glucocorticoid-induced osteonecrosis of the femoral head in rat. *Phytother Res*. 2021;35(5):2824–2835.

47. **Glynn NW**, **Meilahn EN**, **Charron M**, **Anderson SJ**, **Kuller LH**, **Cauley JA**. Determinants of bone mineral density in older men. *J Bone Miner Res*. 1995;10(11):1769–1777.

48. **Hoidrup S**, **Gronbaek M**, **Gottschau A**, **Lauritzen JB**, **Schroll M**, **Copenhagen Centre for Prospective Population Studies**. Alcohol intake, beverage preference, and risk of hip fracture in men and women. *Am J Epidemiol*. 1999;149(11):993–1001.

49. **Al-Hourani K**, **Tsang S-T**, **Simpson A**. Osteoporosis: current screening methods, novel techniques, and preoperative assessment of bone mineral density. *Bone Joint Res*. 2021;10(12):840–843.

50. **Zhao D-W**, **Ren B**, **Wang H-W**, **et al**. 3D-printed titanium implant combined with interleukin 4 regulates ordered macrophage polarization to promote bone regeneration and angiogenesis. *Bone Joint Res*. 2021;10(7):411–424.

51. **Liu C**, **Castillo AB**. Targeting osteogenesis-angiogenesis coupling for bone repair. *J Am Acad Orthop Surg*. 2018;26(7):e153–e155.

52. **Cao Y**, **Gong Y**, **Liu L**, **et al**. The use of human umbilical vein endothelial cells (HUVECs) as an in vitro model to assess the toxicity of nanoparticles to endothelium: a review. *J Appl Toxicol*. 2017;37(12):1359–1369.

53. **Xiong J**, **Onal M**, **Jilka RL**, **Weinstein RS**, **Manolagas SC**, **O'Brien CA**. Matrix-embedded cells control osteoclast formation. *Nat Med*. 2011;17(10):1235–1241.

54. **Zelzer E**, **Mamluk R**, **Ferrara N**, **Johnson RS**, **Schipani E**, **Olsen BR**. VEGFA is necessary for chondrocyte survival during bone development. *Development*. 2004;131(9):2161–2171.

55. **Cheng P**, **Chen C**, **He H-B**, **et al**. miR-148a regulates osteoclastogenesis by targeting V-maf musculoaponeurotic fibrosarcoma oncogene homolog B. *J Bone Miner Res*. 2013;28(5):1180–1190.

56. **Li X**, **Xie W**, **Xie C**, **et al**. Curcumin modulates miR-19/PTEN/AKT/p53 axis to suppress bisphenol A-induced MCF-7 breast cancer cell proliferation. *Phytother Res*. 2014;28(10):1553–1560.

57. **Li J**, **Yang S**, **Yan W**, **et al**. MicroRNA-19 triggers epithelial-mesenchymal transition of lung cancer cells accompanied by growth inhibition. *Lab Invest*. 2015;95(9):1056–1070.

58. **Jiang X-M**, **Yu X-N**, **Liu T-T**, **et al**. microRNA-19a-3p promotes tumor metastasis and chemoresistance through the PTEN/Akt pathway in hepatocellular carcinoma. *Biomed Pharmacother*. 2018;105:1147–1154.

59. **Tan Y**, **Yin H**, **Zhang H**, **et al**. Sp1-driven up-regulation of miR-19a decreases RHOB and promotes pancreatic cancer. *Oncotarget*. 2015;6(19):17391–17403.

60. **Chen W**, **Zheng R**, **Baade PD**, **et al**. Cancer statistics in China, 2015. *CA Cancer J Clin*. 2016;66(2):115–132.

61. **Culafić D**, **Djonic D**, **Culafic-Vojinovic V**, **et al**. Evidence of degraded BMD and geometry at the proximal femora in male patients with alcoholic liver cirrhosis. *Osteoporos Int*. 2015;26(1):253–259.

62. **Callaci JJ**, **Himes R**, **Lauing K**, **Wezeman FH**, **Brownson K**. Binge alcohol-induced bone damage is accompanied by differential expression of bone remodeling-related genes in rat vertebral bone. *Calcif Tissue Int*. 2009;84(6):474–484.

63. **Wang Q-S**, **He R**, **Yang F**, **et al**. FOXF2 deficiency permits basal-like breast cancer cells to form lymphangiogenic mimicry by enhancing the response of VEGF-C/VEGFR3 signaling pathway. *Cancer Lett*. 2018;420:116–126.

64. **Wang Q-S**, **Kong P-Z**, **Li X-Q**, **Yang F**, **Feng Y-M**. FOXF2 deficiency promotes epithelial-mesenchymal transition and metastasis of basal-like breast cancer. *Breast Cancer Res*. 2015;17(1):30.

65. **Nik AM**, **Reyahi A**, **Pontén F**, **Carlsson P**. Foxf2 in intestinal fibroblasts reduces numbers of Lgr5(+) stem cells and adenoma formation by inhibiting Wnt signaling. *Gastroenterology*. 2013;144(5):1001–1011.

66. **Alvisa-Negrín J**, **González-Reimers E**, **Santolaria-Fernández F**, **et al**. Osteopenia in alcoholics: effect of alcohol abstinence. *Alcohol Alcohol*. 2009;44(5):468–475.

67. **Nyquist F**, **Berglund M**, **Nilsson BE**, **Obrant KJ**. Nature and healing of tibial shaft fractures in alcohol abusers. *Alcohol Alcohol*. 1997;32(1):91–95.

68. **Pepersack T**, **Fuss M**, **Otero J**, **Bergmann P**, **Valsamis J**, **Corvilain J**. Longitudinal study of bone metabolism after ethanol withdrawal in alcoholic patients. *J Bone Miner Res*. 1992;7(4):383–387.

69. **Nyquist F**, **Halvorsen V**, **Madsen JE**, **Nordsletten L**, **Obrant KJ**. Ethanol and its effects on fracture healing and bone mass in male rats. *Acta Orthop Scand*. 1999;70(2):212–216.

Author information:
- D. Zhu, PhD, Orthopedic Surgeon
- H. Fang, MD, Orthopedic Surgeon
- P. Liu, MD, Orthopedic Surgeon
- Q. Yang, MD, Orthopedic Surgeon
- P. Luo, PhD, Orthopedic Surgeon
- Y. Gao, PhD, Orthopedic Surgeon
- Y-X. Chen, MD, Orthopedic Surgeon
  Department of Orthopedic Surgery, Shanghai Jiao Tong University Affiliated Sixth People's Hospital, Shanghai, China.
- H. Yu, MD, Orthopedic Surgeon, Department of Orthopedic Surgery, The First Affiliated Hospital of Xiamen University, Xiamen, China.
- C. Zhang, PhD, Professor, Department of Orthopedic Surgery, Shanghai Jiao Tong University Affiliated Sixth People's Hospital, Shanghai, China; Institute of Microsurgery on Extremities, Shanghai Jiao Tong University Affiliated Sixth People's Hospital, Shanghai, China.

Author contributions:
- D. Zhou: Writing – review & editing, Conceptualization.
- H. Fang: Investigation, Writing – original draft.
- H. Yu: Investigation, Writing – original draft.
- P. Liu: Validation.
- Q. Yang: Validation.
- P. Luo: Visualization.
- C. Zhang: Supervision.
- Y. Gao: Supervision.
- Y-X. Chen: Writing – review & editing.

- D. Zhu and H. Fang contributed equally to this work.